Improving Soft Pneumatic Actuator Fingers through Integration of Soft Sensors, Position and Force Control, and Rigid Fingernails

John Morrow[1], Hee-Sup Shin[2], Jacob Torrey[1], Riley Larkins[1], Steven Dang[1], Calder Phillips-Grafflin[1], Yong-Lae Park[2], and Dmitry Berenson[1]

***Abstract*— Soft Pneumatic Actuators (SPAs) have recently become popular for use as fingers in robotic hands because of their inherent compliance, low cost, and ease of construction. We seek to overcome two key limitations which limit SPAs' abilities to grasp and manipulate objects: 1) Current SPAs lack position or force sensor feedback, which prevents controlling them precisely (e.g. to achieve a hand preshape or apply a specified pushing force), and 2) the tip of the SPA is compliant and has high friction against common surfaces, causing the SPA to stick against surfaces when grasping objects from above. To overcome the first limitation we propose methods to integrate soft eGaIn sensors into SPAs and controllers that use these sensors' feedback for position and force control. To overcome the second limitation, we explore ways to embed rigid fingernails into the tip of the SPA so that the finger does not stick against surfaces and can wedge itself under objects. Our experiments suggest that we can achieve low steady-state error and overshoot in position and force using feed-forward models that relate pressure, force, and curvature along with a PID controller. We also compare several fingernail designs and show that the best-performing design significantly outperforms having no fingernails when grasping a set of common objects from a table.**

I. INTRODUCTION

Soft robotics is becoming a more prevalent field of the research within the robotics community; however, the majority of research is focused on the mechanical structure of actuators and other soft systems. Two less-explored areas of soft robotics consist of the integration of sensing systems with soft robots and the integration of rigid components with soft systems. Both of these kinds of integration have the potential to greatly impact the performance of soft actuators, specifically the Soft Pneumatic Actuator (SPA) [7], [13], [2]. The improvements to the SPA discussed in this work are oriented towards using the actuators as fingers in a gripper.

The integration of sensing systems enables precise closed-loop force and position control to be performed on the SPA. Many current SPAs rely on the control of the pressure inside the actuators to control the actuator position, but do not have feedback as to the actual position of the actuator or the force it applies to objects. Rigid force and position sensors are readily available, but integrating them into a soft system is difficult because they limit the compliance of the actuator. With the recent development of deformable eGaIn sensors [14], it is now possible to embed soft position and force senors into the SPA which do not disturb the compliance of the actuator. We propose a method to integrate these sensors into SPAs as well as controllers that use feed-forward models of these sensors to precisely control the position and force applied. We are not aware of previous work which can control the force and position of the type of SPAs used in this work with integrated sensors.

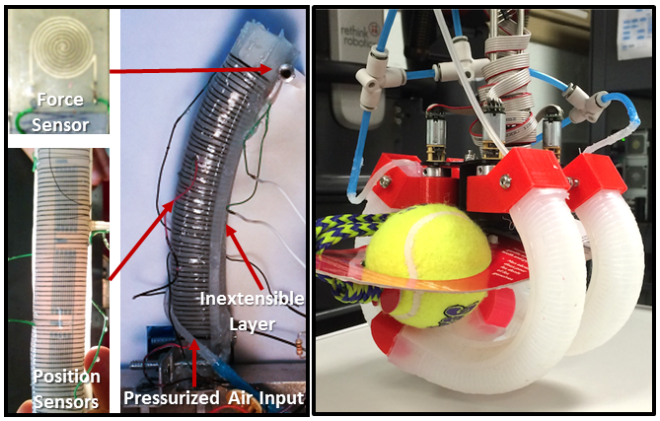

Fig. 1: Left: The components of our SPA. The sensors are soft eGaIn sensors. Right: SPAs with our proposed fingernails used as part of a hand.

However, compliance in every part of the SPA is not always desirable. When used for grasping objects from above, the SPA can make contact with the surface the object is resting on. We found that this contact often causes the SPA to stick to the surface (due to high friction and compliance) and thus the grasp fails. Combining rigid "fingernails" with SPAs will improve grasping performance without compromising the useful deformation properties of the actuator. In this work we evaluate several fingernails for use with the SPA on objects with varying contact surfaces with a table. We show that some fingernails lead more often to the object being scooped inside the arc of the SPA, which is more likely to result in a power grasp. We also show that the best-performing fingernail design outperforms the standard SPA when grasping objects from a table.

The contributions of this paper are: 1) Methods to integrate soft position and force sensors with SPAs; 2) Force and position controllers for SPAs with an optional force limit; and 3) Fingernail designs that improve success rate of grasps off of flat surfaces.

The rest of this paper will detail related work, embedding eGaIn sensors, using their feedback for control, fingernail design, and results showing the efficacy of the controllers and the fingernails.

[1]Worcester Polytechnic Institute
[2]Carnegie Mellon University

II. RELATED WORK

SPAs have undergone many changes since their initial development by Galloway et al [7]. Mosadegh et al. designed the PneuNet actuator [13], which uses multiple small air chambers instead of the single chamber design used by Galloway. Deimel and Brock [2] adapted Galloway's actuator to make the PneuFlex actuator, which is the basis for the actuator we use in our work.

Though SPAs are a popular choice for compliant fingers, alternative compliant hand designs exist. The SDM gripper, featured under-actuated fingers with embedded soft material 'ligaments' to allow compliance [3]. Though the joints of these fingers are compliant, the links are rigid. In this work we seek fingers that can comply to arbitrary geometry and disturbances, so we focus on SPAs.

Precise control of soft actuators is a relatively new field of study, and there has been limited work done on the subject. Most approaches have used the Finite Element Method to control soft systems and have heavy emphasis on modeling the kinematics and dynamics of actuators[5][8][12]. Through modeling the dynamics of the pneumatic networks, precise control can be achieved, but it does not take into account the interaction between the actuator and its environment. Also, we seek a real-time controller and solving FEM accurately is not practical in real time. Other approaches attempt to emulate natural behaviors of tentacles and other natural continuum actuators[17]. The approach used in our work takes advantage of having sensors embedded in the actuators, and empirically models the actuator responses.

In this work we use EGaIn sensors developed by Park et al. [14]. These sensors have been applied to a lower limb motion sensing suit which used them to detect gaits [11]. These senors were also embedded inside fabric [18]. However, to our knowledge, these kinds of sensors have not previously been used for feedback inside a soft actuator.

A key component of our design is the rigid fingernails that can be used to wedge under objects. Loh and Tsukagoshi designed a multi-stage soft actuator to lift the elderly from beds. To get underneath the human, Loh and Tuskagoshi implemented a 'slip-in tip', which is a metal plate that rolls between the body and the bed [10]. The actuator design is similar to ours, however we aimed for a passive system to get underneath objects (i.e. a fingernail).

Using rigid fingernails with SPAs requires bonding hard and soft components together. Kwok et al. [9] proposed using NbFeB ring magnets for such an interface. In our approach we integrate the rigid components into the soft material using a porous anchor, which is both low-cost and able to withstand significant external forces.

III. PROPRIOCEPTION WITH SOFT SENSORS

SPAs typically have no feedback other than the pressure in the actuators, which does not map directly to position or force. To improve the performance of the actuator through precise force and position control, we introduced more sensor feedback into the system. Specifically, we used EGaIn sensors, which are deformable and are able to measure the force applied by, and the curvature of, the actuator. The specific circuitry used in the sensing is discussed in [14]. We describe how these sensors are built below.

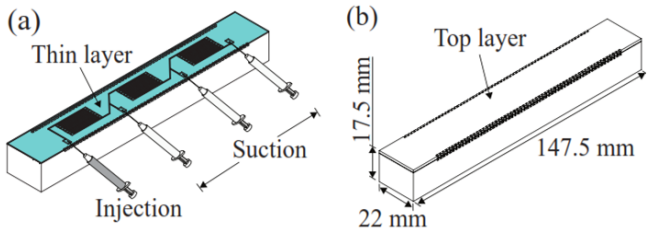

Fig. 2: (a) EGaIn injection process for three soft strain sensors and (b) final assembly of SPA.

A. Force sensing

The gripping force of the SPA can be measured using soft pressure sensors at the tip, made from silicone. When force is applied to the tip, it deforms the embedded microchannels filled with EGaIn of the soft sensor, causing an increase in the electrical resistance of the microchannels. In this sensor, we chose a spiral microchannel pattern, as shown in Fig. 1, to prevent the sensor from having directional strain sensitivity.

The microfluidic soft sensors were individually fabricated using a layered molding and casting process described in [14]. Two different 3-D printed molds (one with a microchannel pattern, the other with a flat surface) were prepared first, and a platinum cure silicone rubber (Dragon Skin 10, Smooth-On) was poured in the mold and cured. The two cured layers were bonded by spin-coating the same uncured silicone material on the flat layer. Before the silicone coat was cured, the microchannel layer was carefully laminated on top of the flat layer. Finally, EGaIn was injected using a 25 ga hypodermial syringe needle.

B. Position sensing

The position (or shape) of the SPA can be detected using soft strain sensors in the SPA structure. Differently from the force sensors, the strain sensors were directly embedded during the fabrication of the SPA. The mold for the SPA contains three strain sensor patterns. Only the top layer was separately cast and laminated on the sensor side of the finger. Since the same silicone material was used for the sensor, the sensor structure did not cause any property changes of the finger structure. Each finger contains three strain sensors for detecting the shape of the finger in three different locations. Since all three sensors were connected in series, a single injection was able to fill the entire microchannel. Fig. 2 shows the EGaIn injection process for filling all three sensors simultaneously. While one syringe at the bottom injects EGaIn, the other three remove the captured air during fabrication.

The straight serpentine pattern, which can be easily seen in regular strain gauges, facilitates increase of directional strain sensitivity in the axis of the long microchannels. Since the strain sensors were located off the neutral axis, the bending of the finger could be easily measured by monitoring the

strain changes on the sensors. Fig. 1 shows the configuration of the position and force sensors.

IV. Force and Position Control

Position and force feedback from the soft sensors enabled several forms of closed loop control. The sensor detecting compression at the actuator tip provides feedback as to the force the actuator is applying to an object, and allows for precise control of the applied force. The sensors embedded in the extensible layer of the actuators allow for curvature feedback and control. We implemented three types of controllers using these sensors: a force controller, a position controller, and a maximum-force position controller. Each controller output is taken as an input to a pressure controller, which utilizes a pressure transducer, allowing for precise monitoring and control of the pressure inside the actuator (see Figure 4.

All the controllers that were used in this research are of the PID + feed-forward form. Using an accurate model in a feed-forward term reduces how much compensation the PID components are responsible for, resulting in improved controller performance. Using the instrumented actuators, empirically generated feed-forward terms were able to be introduced in the control logic. The piece-wise functions that define the feed forward terms are calculated by applying the Ramer-Douglas-Peucker Algorithm to the calibration data [4]. With this algorithm the number of line segments is variable, as it will continue to add segments until the maximum error between the linear approximations and the actual data is below a predefined threshold.

A. Pressure Control

The pressure in the actuators is controlled by using a PWM-driven solenoid valve, connected to a pressure regulator, filter, and air compressor. The PWM signal for the solenoids is commanded by the pressure controller, and the solenoids are driven at 50 Hz. This controller consists of a PID loop and a feed-forward term. The model used for the feed-forward term was developed empirically by recording the duty cycles and the corresponding pressure transducer readings. The curve generated from this relationship is then approximated as a piecewise linear function. This approximation is sufficiently accurate, and reduces the computational load in the controller logic. An example calibration curve is shown in Figure 3a. The resulting equation is shown in Equation 1. This is the first of the calibration steps for the controller system.

$$D_{expected} = \begin{cases} m_0 p_{desired} + b_0 & : 0 < p_{desired} < t_0 \\ m_1 p_{desired} + b_1 & : t_0 < p_{desired} < t_1 \\ \vdots & \vdots \\ m_n p_{desired} + b_n & : t_n < p_{desired} \end{cases} \tag{1}$$

$D_{expected}$ is the duty cycle output of the pressure controller feed-forward term, m and b are the slope and offset of each line from the piecewise linear model, $p_{desired}$ is the commanded pressure, and t is the threshold for the range of

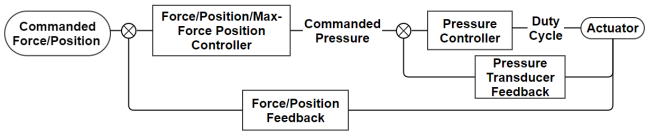

Fig. 4: Controller system block diagram. The force, position, and maximum-force controller outputs are passed into the pressure controller. All the sensors are located on the actuator.

desired values. The full pressure controller equation is shown in Equation 2.

$$E_p = P_{desired} - P_{current} \tag{2a}$$

$$p_p = k_p E_p \tag{2b}$$

$$i_p = \alpha i_p' + k_i E_p \Delta t \tag{2c}$$

$$d_p = k_d \frac{E_p - E_p'}{\Delta t} \tag{2d}$$

$$D = p_p + i_p + d_p + D_{expected} \tag{2e}$$

E_p is the error between the desired, $P_{desired}$, and current, $P_{current}$, pressures. The p_p, i_p, and d_p terms are the proportional, integral, and derivative terms in the controller. Each of these terms has a constant, k, and the terms are summed with the feed-forward term to yield the duty cycle, D. The $'$ superscript refers to the value of that variable at the previous time step. The time between each interation of the control loop is Δt. The α used in the integral term is a constant that helps prevent integral windup. The following three controllers command the desired pressure, which is the input of this controller. A diagram of how the controllers are integrated together is shown in Figure 4.

B. Force Control

The force controller once again is a PID + feed-forward controller. The feed-forward term is comprised of a term generated by modeling the force, and a term dependent on the position of the actuator. The position of the actuator contributes a large portion of the feed-forward term, and was introduced to allow the force controller to operate independently of position. The model of the force is generated by observing the relationship between applied force and pressure, and the position term is solely dependent on the actuator position at the time of contact with the object. The relationships and resultant approximations can be seen in Figure 3c, and the equation used in this work can be seen in Equation 3b. Finding these terms is the second calibration step, which is completed by repeatedly applying forces to an object in the path of the actuator, and recording the force, position, and pressure sensor readings. The position readings are used to compensate for the position at which the force sensor makes contact with the object, isolating the pressure required to apply the force. The pressure to force relationship then yields the force feed-forward term.

It was also determined in the design of the controllers that the actuators operate with two different modes of actuation. Increasing the pressure in the actuator was deemed to be "positive actuation," and decreasing the pressure was

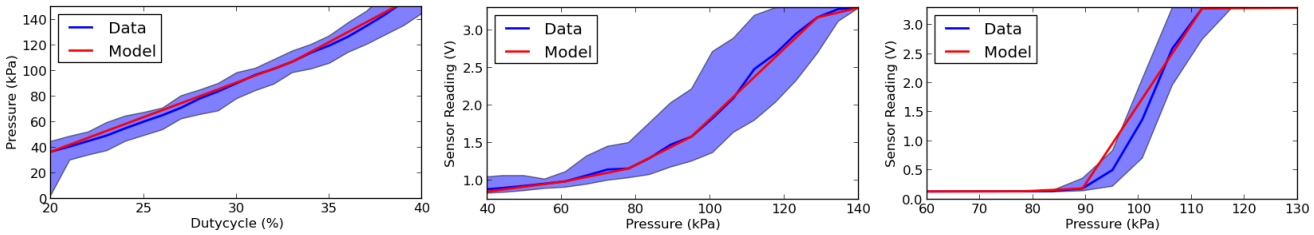

(a) Pressure sensor calibration. (b) Position sensor calibration. (c) Force sensor calibration.

Fig. 3: Calibration curves for the controllers. The red 'model' line is the approximated curve, the blue shaded 'data' area is the range of measured values from multiple trials, and the dark blue 'data' line is the average of the shaded region.

"negative actuation." The maximum rate at which pressure in the actuator can be increased is determined by the external supply pressure. When pressure is decreased, only the elasticity of the silicone returns the actuator to its unpressurized position. To compensate for this, two different sets of PID gains were found, one for positive actuation, and one for negative actuation.

Through testing of the controller, it was determined that the integral term was responsible for large overshoot, which was resolved by resetting the integral term when the commanded value changed more than 5% of the full sensor range. In testing it was found that using 5% of the full sensor range as the threshold would reduce the overshoot without increasing the rise time of the controller.

$$p_{expected,f} = \begin{cases} m_0 f_{desired} + b_0 & : 0 < f_{desired} < t_0 \\ m_1 f_{desired} + b_1 & : t_0 < f_{desired} < t_1 \\ \vdots & \vdots \\ m_n f_{desired} + b_n & : t_n < f_{desired} \end{cases} \tag{3a}$$

$$p_{expected,P} = \begin{cases} m_0 P_{current} + b_0 & : 0 < P_{current} < t_0 \\ m_1 P_{current} + b_1 & : t_0 < P_{current} < t_1 \\ \vdots & \vdots \\ m_n P_{current} + b_n & : t_n < P_{current} \end{cases} \tag{3b}$$

$$E_f = f_{desired} - f_{current} \tag{3c}$$

$$p_f = \begin{cases} k_{p,pos} E_f & : 0 < E_f \\ k_{p,neg} E_f & : 0 > E_f \end{cases} \tag{3d}$$

$$i_f = \begin{cases} \alpha i'_f + k_{i,pos} E_f \Delta t & : 0 < E_f \\ \alpha i'_f + k_{i,neg} E_f \Delta t & : 0 > E_f \end{cases} \tag{3e}$$

$$d_f = \begin{cases} k_{d,pos} \frac{E_f - E'_f}{\Delta t} & : 0 < E_f \\ k_{d,neg} \frac{E_f - E'_f}{\Delta t} & : 0 > E_f \end{cases} \tag{3f}$$

$$u_f = p_f + i_f + d_f + p_{expected,f} + p_{expected,P} \tag{3g}$$

The $p_{expected,f}$, and $p_{expected,P}$ terms are the force and position feed-forward terms. The E_f term is the difference between the commanded force, $f_{desired}$, and the force sensor reading, $f_{current}$. The subscripts, pos, and neg, of the k_p, k_i, and k_d constants denote whether the gain is used for positive or negative actuation. The final output u_f is pressure that is used as an input in the pressure controller.

C. Position Control

The position controller incorporates the feedback from the curvature sensors embedded in the extensible layer of the actuators. There are three sensors providing feedback, and constant curvature in the actuator is assumed, a common assumption in previous work[2]. The three curvature sensor readings are averaged to generate the curvature reading. The feed-forward term is generated by finding the relation between the averaged curvature sensor reading and pressure. This position feed-forward term is dependent on the desired position of the actuator, unlike the term in the force controller that uses the current actuator position. The calibration curves and equations are the same form as those used in the force controller, and are shown in Figure 3b, and Equation 4a.

$$p_{expected} = \begin{cases} m_0 P_{desired} + b_0 & : 0 < P_{desired} < t_0 \\ m_1 P_{desired} + b_1 & : t_0 < P_{desired} < t_1 \\ \vdots & \vdots \\ m_n P_{desired} + b_n & : t_n < P_{desired} \end{cases} \tag{4a}$$

$$E_P = P_{desired} - P_{current} \tag{4b}$$

$$p_P = \begin{cases} k_{p,pos} E_P & : 0 < E_P \\ k_{p,neg} E_P & : 0 > E_P \end{cases} \tag{4c}$$

$$i_P = \begin{cases} \alpha i'_P + k_{i,pos} E_P \Delta t & : 0 < E_P \\ \alpha i'_P + k_{i,neg} E_P \Delta t & : 0 > E_P \end{cases} \tag{4d}$$

$$d_P = \begin{cases} k_{d,pos} \frac{E_P - E'_P}{\Delta t} & : 0 < E_P \\ k_{d,neg} \frac{E_P - E'_P}{\Delta t} & : 0 > E_P \end{cases} \tag{4e}$$

$$u_P = p_P + i_P + d_P + p_{expected} \tag{4f}$$

D. Maximum-Force Position Control

In the maximum-force position controller, the force feedback and position controller are combined. Controlling the position is the primary function of this controller, but it will limit the force applied by the actuator to ensure the safety of an object in contact with the actuator. When the actuator makes contact with an obstacle, the force feedback will prevent the controller from increasing the actuator force past the specified level, allowing for safe manipulation at any position. As the force feedback approaches the specified threshold, the output of the position controller is attenuated. While the position control signal is being attenuated, a

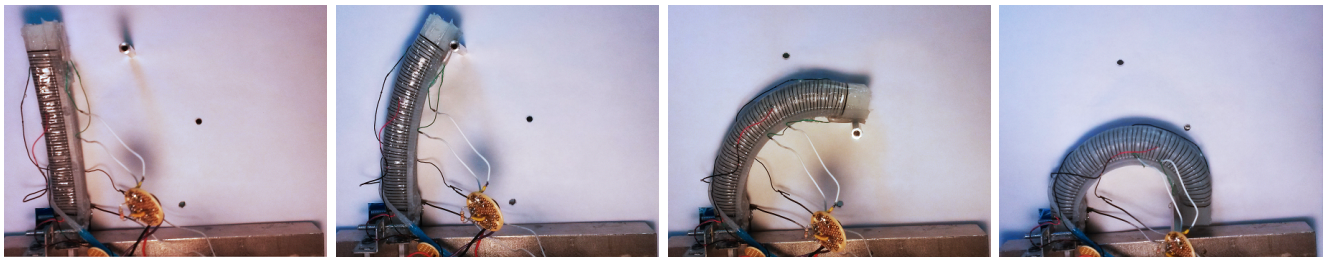

Fig. 5: Actuator at unpressurized position (left-most) and the three obstacle positions (positions 1-3, left to right) used for the force control testing.

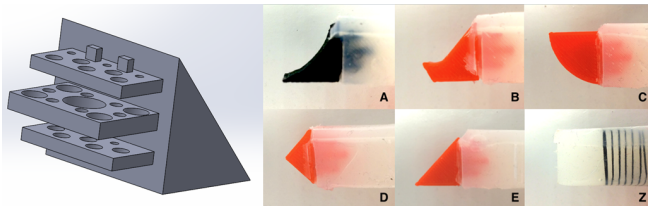

Fig. 6: Left: Anchor design. Right: Set of fingernail designs.

complementary weighting function is applied to the same feed-forward term used in the force controller. This feed-forward term accounts for both position and force, and can sufficiently approximate the necessary pressure to hold the actuator at or below the threshold force. The equation for this controller is shown below.

$$u = (p_P + i_P + d_P + p_{expected})(1 - e^{-K_g E_f}) + \gamma(p_{expected,P} + p_{expected,f})(e^{-K_g E_f}) \quad (5)$$

The E_f term is the difference between the specified force threshold and the force sensor reading. The constant K_g was found empirically, and is used to control how rapidly the transition between the position controller and the force control term occurs. The γ is used to account for error in the estimation by scaling the force feed-forward term.

V. Fingernail Integration and Design

Our other contribution to create more versatile SPAs was to embed rigid fingernails into the soft material. At the back of each fingernail is a set of three anchor protrusions. These protrusions have a pattern of holes with varying sizes. These fingernail anchors were designed to withstand forces pulling the anchor horizontally out of the finger, as well as moments on the fingernail when in contact with the table. In order to keep an even dispersal of force on the silicone inside each hole, we made them into a circular shape (see Figure 6).

1) Fingernail Design: We selected several wedge primitives inspired by other structures designed to slide underneath objects (see Figure 6). Design A is inspired from a dustpan, B is inspired from a badger's claws, C is inspired from similar fingertips by Soft Robotics Inc., D is a wedge design, and E is an inclined plane. For comparison, a bare finger is also shown in Figure 6.

The dustpan design was chosen for its simplicity. Contrary to a dustpan's dull tip, we gave this fingernail design a sharp thin wedge in line with the dustpan's design. We added a slope along the tip of the finger to help guide objects onto the finger's passive layer. The badger claw design was inspired from the digging methods of badgers. To dig, badgers use their claws, which are also conveniently designed to get behind objects, such as rocks found in their digging paths. We theorized that this nail design would get underneath objects [16]. The Soft Robotics Inc. finger-tips were inspired from promotional videos of their soft robotic gripper [15]. In the video, simple finger caps were added to the tips of the fingers to improve a precision grasp on an object. We modified the idea in way we thought would aid a power grasp. Finally, we chose to include the simple wedge fingernail design to see if a simple design would suffice. We tried two different wedge styles: one with the point in the center of the fingertip, nail D, and another in the style of an incline plane, nail E. Evaluations of these designs are presented in the following section.

VI. Results

A. Controller evaluation

The force controller k_p, k_i, and k_d gains were 80, 90, 0.5 for positive actuation, and 25, 5, and 0.5 for the negative actuation. The position controller k_p, k_i, and k_d gains were 75, 100, and 0.5 for positive actuation, and 75, 175, and 0.5 for negative actuation. The gains for the pressure controller were 5, 1, and 0.5. All controllers had a values of 0.994 for α and 10 ms for Δt. For the feed-forward term line segments, the force term only used one line segment, whereas the position and pressure feed-forward terms used four line segments each (see Figure 3).

The performance of the three controllers was measured by observing responses to step and ramp inputs. The tests for the force controller consisted of driving the sensor into a rigid obstacle and measuring the applied force (see the setup in Figure 5). The controller had different responses depending on the level of pressure in the actuator, and so was tested at three different positions. The results of the step and ramp responses can be found in Figures 7 and 8. Some notable results of the force responses were the relatively fast rise times, and low steady state errors. The rise times over the responses in Figure 7(left) were 88ms on average, and the steady state error averaged 5.4% of the step change. The maximum overshoot was 22.8% of the step size, but overshoot only occurred on the final steps of this range of pressures. These numbers were calculated from four trials at position 1, with 10 step inputs for each trial.

The position controller was put through a similar set of tests, only removing the obstacle to allow the actuator to be

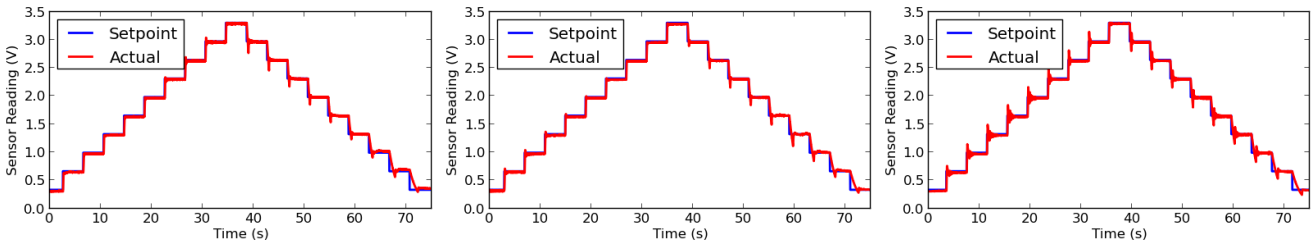

Fig. 7: Force control step responses. Each step is 10% of the total measurable force range. Left-Right: Positions 1-3. Note the increase in overshoot and settling time at Position 3.

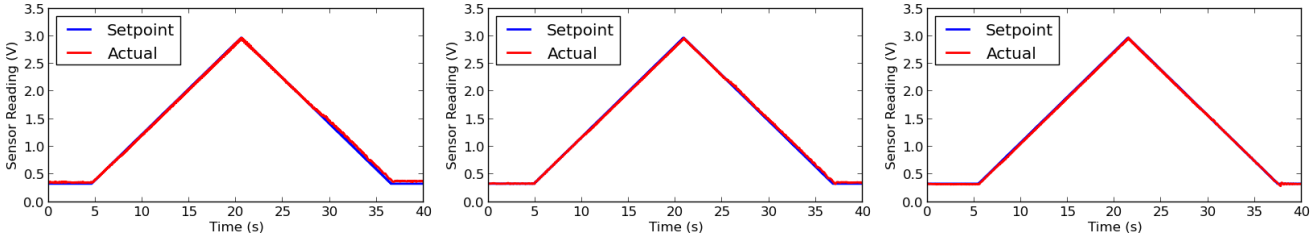

Fig. 8: Force control ramp responses. Left-Right: Positions 1-3.

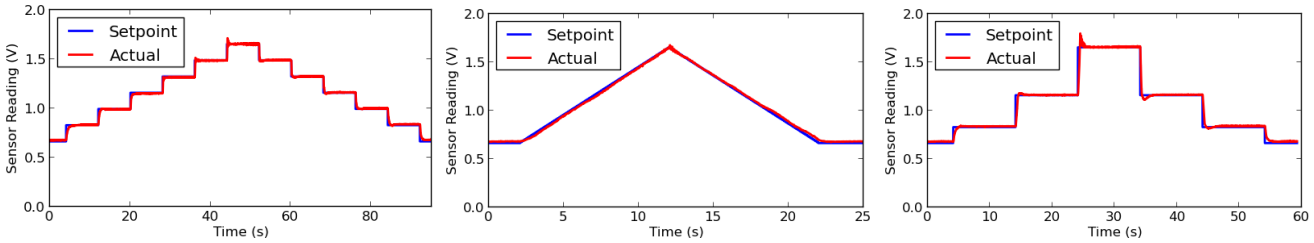

Fig. 9: Position control responses. Left-Right: Positions 1-3.

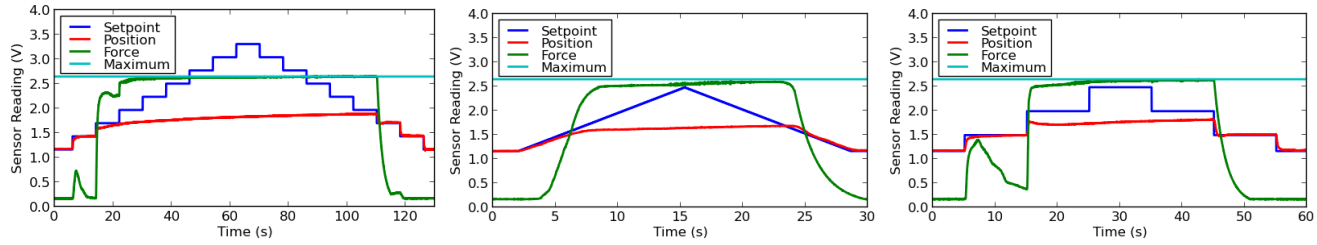

(a) Position controller step responses (b) Position controller ramp response (c) Position controller large step responses

Fig. 10: Maximum-force position control at Position 1. The maximum force was held constant throughout the trials.

unobstructed as it moved through the commanded positions (see Figure 9). The average rise time for the responses in Figure 9(left) was 380ms, the steady state error was 3% of the step size, and the maximum overshoot was 36% of the step size. In general, the position controller was not as susceptible to the hysteresis of the sensors/actuators.

For the maximum-force position controller, the same set-points as for the position controller were used, but the obstacle from the force control tests was put at position 1. Through these tests we confirmed that using our method the controller would not drive the actuator past the force threshold. The force threshold was set to an arbitrary force value, and $\gamma = 0.95$, and $K_g = 6$. For all tests the force remained below the threshold (see Figure 10). Demonstrations of this controller are shown in the attached video.

B. Fingernail evaluation

Two tests were used to determine the best fingernail design from the set of fingernail designs. The first tested the fingernails in a controlled setting. The second test used these fingernail designs on an end effector to test its performance on a realistic grasping task. We have provided results for each test separately in this section.

1) Test on Surface Contact Edges: The effectiveness of each fingernail was tested on a small sample size of surface edges. To do this, a variety of 3D printed boxes were created with varying surface flushness, which is the interface between the outer edge of the object and the surface it is resting on, shown in Figure 11. In this first test a single finger was used to test whether the nails could get underneath and lift the test objects, which were located underneath the

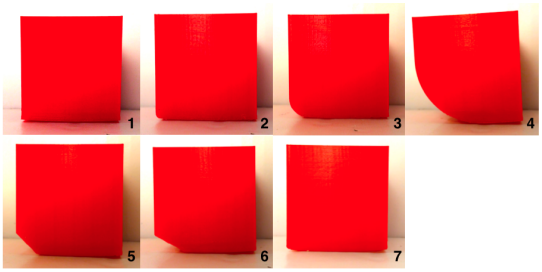

Fig. 11: Set of test objects for fingernail experiments.

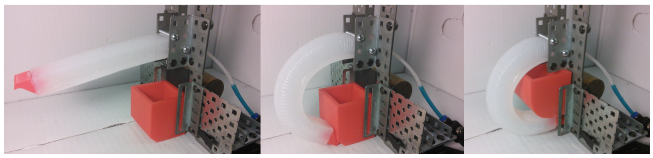

Fig. 12: Test setup for the single finger fingernail test. Test objects are placed underneath the finger (left). A successful grasp is shown on the right. In some cases a nail will wedge underneath an object but the finger does not lift it (center).

finger. The pressure in the finger was increased to 22 PSI and the resulting grasp would be observed. 22 PSI was used because higher pressures would cause too much curvature for the rig. This test was designed to determine if the nail has any potential to get underneath objects, so the object was constrained to vertical movement.

A successful grasp in this test was defined as one that lifted the object and brought it into contact with the passive layer of the finger. The test setup is shown in Figure 12. The results are shown in Table I. The best performing fingernail from this experiment was found to be nail C. Looking at the data, we chose this fingernail because it had the highest number of successful grasps. Some fingernails showed a higher potential, evident in their high numbers of partially successful grasps such as nails D and A, respective to performance. We chose to use nails C, D, and A based on their successes and potential for the next test.

2) Practical Application Experiment: In the second test, a practical application of the fingers was tested. We used a basic 4-finger gripper design (see Figure 1) to evaluate the effectiveness of each fingernail type. This gripper was tested on the Amazon Picking Challenge object set. These 27 objects in Figure 13, ranging from a spark plug to a package of Oreo cookies, would give us an independently determined, wide range of common objects to grasp. The tests on these objects would also verify the feasibility of the actuators in future research and commercial applications.

To verify any performance gain from the fingernails, we designed an experiment where the gripper approaches from above the object to grasp the object off a flat surface. The object was placed on a marked spot where the gripper mounted to the Rethink Robotics' Baxter was positioned over it. The gripper was given a height clearance of five centimeters from finger tip to table surface over each object. The actuators were inflated to a constant 22 PSI, which would supply adequate gripping force for all objects tested. After the object was grasped, Baxter would raise the object

	Objects						
Nails	1	2	3	4	5	6	7
A							
B							
C							
D							
E							
Z							

TABLE I: Single finger fingernail test results. Red: failure to get under object, green: success, yellow: the fingernail slipped under the object but was unable to successfully lift the object.

Fig. 13: Amazon Picking Challenge objects

and execute a predefined "shaking" trajectory to test the reliability of the grasp. If the object fell out of the hand at any point, that trial was marked as a failure. We conducted five trails for each object, if 4 or more trials succeeded we deemed the object graspable by the hand. Results for all objects are summarized in Table II.

Using the bare fingers, the gripper was able to grasp 12 of the 27 objects (44%) with at least an 80% success rate. The nail C design improved over the bare finger by one more successfully grasped object, resulting in 48.1% of objects grasped. The nail A design had a better improvement with 59.3% of objects grasped. However, the best improvement over the bare finger was with the nail D design, which allowed the hand to grasp 77.8% of objects. Selected trials from the fingernail tests can be seen in the attached video.

VII. DISCUSSION

Control: All three controllers have much less overshoot and error when operating over lower pressures. It was clear from the results of these tests that the actuators are more difficult to precisely control at high pressures. This is partially due to the nonlinear relationship between the pressure in the actuator and the curvature of the actuator at higher pressures.

From the different step responses it is also possible to observe the mechanical hysteresis that is present in the actuators. The sensors also have hysteresis, and in both cases it is caused by the deformation of the silicone. In

Bare Finger Results								
1	2	3	4	5	6	7	8	9
10	11	12	13	14	15	16	17	18
19	20	21	22	23	24	25	26	27
Nail A Results								
1	2	3	4	5	6	7	8	9
10	11	12	13	14	15	16	17	18
19	20	21	22	23	24	25	26	27
Nail C Results								
1	2	3	4	5	6	7	8	9
10	11	12	13	14	15	16	17	18
19	20	21	22	23	24	25	26	27
Nail D Results								
1	2	3	4	5	6	7	8	9
10	11	12	13	14	15	16	17	18
19	20	21	22	23	24	25	26	27

TABLE II: Results of practical application. The colors represent the average success over the trials with green being averages equal to or greater than 80% and red being averages less than 80%.

the case of the sensors, the silicone needs to allow the microchannels to refill, as was seen in the work done by Park et al. [14]. The actuator response times are governed by how quickly the pressure can be increased in the actuator, and how quickly the silicone returns to its unpressurized position when the pressure is released. On the falling edges of the force responses in Figure 7, the slower falling time resulted in less undershoot. The maximum undershoot was also correlated with the fastest falling time.

The inspiration for the maximum-force position controller was taken from the PR2 grippers, as they have a built-in force thresholding function [6]. This controller showcases the potential for well-instrumented soft actuators used in manipulation tasks. There are some inconsistencies in the responses, as the force feedback is dependent on the contact between the sensor and the obstacle. If the actuator achieves contact with the obstacle, but the force sensor is not seated ideally on the obstacle, there is the potential for actuators to twist and bend, changing position without changing the force. Similarly, there is potential for the force to change drastically without significant changes in position. This can be best seen in Figure 10c, as the force spikes on initial contact, settles, and then increases until it is near the maximum force when the next step occurs. This is one of the limitations of an underactuated, compliant sensor-actuator system.

Fingernails: Nail designs A and D were the most successful due to key design features: nail A's sharp point and nail D's wedge shape. Nail A's sharp point was able to get under the items and push the item onto the actuator, which led into a successful power grasp. Nail D's wedge shape guided the item onto the SPA passive layer for the gripper to grasp the item. Combining the two by adding a sharp point onto nail D may improve results.

There were some geometries that we found that could not be grasped by the SPAs: rectangular prisms such as the spark plug and the box of pencils. This is mostly due to their relative size compared to the SPAs. The fingers are designed for power grasps, and precision grasps should be used to pick up these objects.

VIII. CONCLUSION

We developed precise position and force control and a fingernail to improve the soft pneumatic actuator for grasping. Our position and force controllers used feedback from embedded eGaIn sensors in the finger. The fingernails were 3D printed and embedded into the tip of the finger through use of a three pronged anchor. We found that several fingernails outperformed the bare finger when grasping objects off a flat surface. We also found that, using PID and feed-forward terms, our controllers could accurately control the position and force applied by the SPA.

REFERENCES

[1] M. Cianchetti, A. Licofonte, C. Laschi, 'Bioinspired Soft Actuation System Using Shape Memory Alloys', Actuators, vol. 3, no. 3, pp. 226-244, 2014.

[2] R. Deimel and O. Brock, 'A Compliant Hand Based on a Novel Pneumatic Actuator, ICRA 2013.

[3] A. Dollar and R. Howe, 'A robust compliant grasper via shape deposition manufacturing', IEEE/ASME Trans. Mechatron., vol. 11, no. 2, pp. 154-161, 2006.

[4] D. Douglas and T. Peucker, 'Algorithms for the Redution of the Number of Points Required to Represent a Digitized Line or its Caricature'; Cartographica, University of Toroto Press, vol. 10, no. 2, pp. 112-122 Dec 1973

[5] C. Duriez, 'Control of Elastic Soft Robots based on Real-Time Finite Element Method', ICRA 2013.

[6] 'Force Control with the PR2 Gripper', www.ros.org

[7] K. Galloway, P. Polygerinos, C. Walsh, and R. Wood, 'Mechanically Programmable Bend Radius for Fiber-Reinforced Soft Actuators', ICRA, 2013.

[8] R. Kang, D. Branson, T. Zheng, E. Guglielmino, and D. Caldwel, 'Design, modeling and control of a pneumatically actuated manipulator inspired by biological continuum structures', IOP Publishing, Bioinspiration & Biomimetics, Published 15 July 2013.

[9] S. Kwok, S. Morin, B. Mosadegh, J.-H. So, R. Shepherd, R. Martinez, B. Smith, F. Simeone, A. Stokes, and G. Whitesides, 'Magnetic Assembly of Soft Robots with Hard Components', Advanced Functional Materials, vol. 24, no. 15, pp. 2180-2187, 2013.

[10] C. Loh and H. Tsukagoshi, 'Pneumatic Big-hand Gripper with Slip-in Tip Aimed for the Transfer Support of the Human Body', ICRA, 2014.

[11] Y. Meng, Y.-L. Park, L. Stirling, E. Martinez-Villalpando, R. Wood, P. Aubin, and C. Walsh, 'Soft Wearable Motion Sensing Suit for Lower Limb Biomechanics Measurements', ICRA, 2013.

[12] B. Mosadegh, A. Mazzeo, R. Shepherd, S. Morin, U. Gupta, I. Sani, D. Lai, S. Takayama, G. Whitesides, 'Control of soft machines using actuators operated by a Braille display'. Lab Chip. 2014 Jan 7, Epub 2013 Nov 6. PubMed PMID: 24196070; PubMed Central PMCID: PMC3880808.

[13] B. Mosadegh, P. Polygerinos,C. Keplinger,S. Wennstedt, R. Shepherd,U. Gupta,J. Shim, K. Bertoldi, C. Walsh, and G. Whitesides, 'Soft Robotics: Pneumatic Networks for Soft Robotics that Actuate Rapidly, Advanced Functional Materials, vol. 24, no. 15, pp. 2109-2109, 2014.

[14] Y.-L. Park, B.-R. Chen, and R. Wood, 'Design and Fabrication of Soft Artificial Skin Using Embedded Microchannels and Liquid Conductors', IEEE Sensors Journal, vol. 12, no. 8, pp. 2711-2718, 2012.

[15] C. Roberts (2014, September 24) Soft Robotics [Online]. Available: http://www.http://softroboticsinc.com/

[16] Scotland's Wildlife: Badgers and Development, Scottish Natural Heritage, Edinburgh, UK, 2014. Found at: http://www.snh.org.uk/pdfs/publications/wildlife/badger.pdf

[17] J. Taghia, A. Wilkening, and O. Ivlev, 'Position Control of Soft-Robots with Rotary-Type Pneumatic Actuators, Robotics'; Proceedings of ROBOTIK 2012; 7th German Conference on, vol. 1, no. 6, pp. 21-22 May 2012

[18] M. Yuen, A. Cherian, J. Case1, J. Seipel, and R. Kramer, 'Conformable Actuation and Sensing with Robotic Fabric', IROS, 2013.